Astrophysical reaction rate for $\alpha(\alpha n, \gamma)^9$Be by photodisintegration

K. Sumiyoshi[a,1], H. Utsunomiya[b,2], S. Goko[b,3], and T. Kajino[c,4]

[a]Numazu College of Technology,

Ooka 3600, Numazu, Shizuoka 410-8501, Japan

[b]Department of Physics, Konan University,

Okamoto 8-9-1, Higashinada-ku, Kobe, Hyogo 658-8501, Japan

[c]National Astronomical Observatory,

Osawa 2-21-1, Mitaka, Tokyo 181-8588, Japan

[1]e-mail: sumi@numazu-ct.ac.jp

[2]e-mail: hiro@konan-u.ac.jp

[3]e-mail: gokou@konan-u.ac.jp

[4]e-mail: kajino@nao.ac.jp

Abstract

We study the astrophysical reaction rate for the formation of ^{9}Be through the three body reaction $\alpha(\alpha n, \gamma)$. This reaction is one of the key reactions which could bridge the mass gap at A = 8 nuclear systems to produce intermediate-to-heavy mass elements in alpha- and neutron-rich environments such as r-process nucleosynthesis in supernova explosions, s-process nucleosynthesis in asymptotic giant branch (AGB) stars, and primordial nucleosynthesis in baryon inhomogeneous cosmological models. To calculate the thermonuclear reaction rate in a wide range of temperatures, we numerically integrate the thermal average of cross sections assuming a two-steps formation through a metastable ^{8}Be, $\alpha + \alpha \rightleftharpoons {}^8$Be(n,$\gamma$)^{9}Be. Off-resonant and on-resonant contributions from the ground state in ^{8}Be are taken into account. As input cross section, we adopt the latest experimental data by photodisintegration of ^{9}Be with laser-electron photon beams, which covers all relevant resonances in ^{9}Be. Experimental data near the neutron threshold are added with γ-ray flux corrections and a new least-squares analysis is made to deduce resonance parameters in the Breit-Wigner formulation. Based on the photodisintegration cross section, we provide the reaction rate for $\alpha(\alpha n, \gamma)$^{9}Be in the temperature range from $T_9 = 10^{-3}$ to $T_9 = 10^1$ (T_9 is the temperature in units of 10^9 K) both in the tabular form and in the analytical form for potential usage in nuclear reaction network calculations. The calculated reaction rate is compared with the reaction rates of the CF88 and the NACRE compilations. The CF88 rate, which is based on the photoneutron cross section for the $1/2^+$ state in ^{9}Be by Berman *et al.*, is valid at $T_9 > 0.028$ due to lack of the off-resonant contribution. The CF88 rate differs from the present rate by a factor of two in a temperature range $T_9 \geq 0.1$. The NACRE rate, which adopted different sources of experimental information on resonance states in ^{9}Be, is 4–12 times larger than the present rate at $T_9 \leq 0.028$, but is consistent with the present rate to within $\pm 20\%$ at $T_9 \geq 0.1$.

1 Introduction

The interplay between nuclear physics and astrophysics is essential to clarify the origin of elements in the Universe. Scenarios of the nucleosynthesis in stars rely on the determination of important nuclear reactions and structures along the reaction path [1]. A long way to create heavy elements starting from light elements (p, n, α) has to pass through the gaps in mass number at A=5 and A=8. The bridge to heavy elements such as ^{12}C invokes slow three-body reactions and then links to heavier elements up to iron elements and beyond. The triple alpha reaction for the formation of ^{12}C is usually the key reaction in stars at the helium burning stage.

In a neutron-rich environment, however, there is an important three-body reaction. If neutrons are abundant enough together with alphas, the formation of ^{9}Be can proceed through the reaction $\alpha(\alpha n, \gamma)$. This reaction followed by ^{9}Be$(\alpha,$n$)^{12}$C can compete with the triple alpha reaction and may dominate over, depending on the astrophysical environment.

The importance of the $\alpha\alpha n$ reaction has been pointed out in the r-process in the hot bubble of a core-collapse supernova [2, 3]. After the core bounce in the supernova, a nascent neutron star is formed at the center. The outer material of this proto-neutron star is heated by intense neutrinos emitted from the proto-neutron star's inside and is ejected as a wind. A high-entropy bubble in this neutrino-driven wind is thought to be an ideal site for the r-process nucleosynthesis. Because of the high temperature and the low density, the matter is dissociated into neutrons and protons once, and they reassemble into light elements, mostly alphas. The nucleosynthesis starts from alphas and remaining neutrons when the temperature decreases below $T_9 \sim 5$ in the expanding matter. Since the triple alpha reaction is too slow at the temperature-density conditions in the hot bubble, the $\alpha\alpha n$ reaction forms a bypass flow connecting to ^{9}Be$(\alpha,$n$)^{12}$C. Therefore, the determination of the reaction rate for the ^{9}Be formation is essential for the initial condition of the r-process, namely, the amounts of seed elements and remaining neutrons. Because of the high entropy (i.e. low density), the three body reaction proceeds slowly, resulting in seed elements with a high neutron-to-seed ratio for a successful r-process up to A=200.

In recent studies of the r-process in the neutrino-driven wind, the importance of this reaction

is more evident. It was shown that the r-process can be successful in the wind flow with a very short expansion time and a moderate entropy [4, 5]. In this rapid expansion, there is essentially no time for the triple alpha reaction to set in and, instead, the $\alpha\alpha n$ reaction becomes again crucial for the r-process. The necessary expansion time is determined in comparison with the reaction time scale of the $\alpha\alpha n$ reaction [4]. A more recent study reveals that the reaction flow can go through the neutron-rich region of light elements in the rapidly expanding wind [6, 7]. Therefore, the competition of the $\alpha\alpha n$ reaction with other bypass reactions in the short expansion time should be carefully considered.

The $\alpha\alpha n$ reaction may play an important role in other astrophysical environments. In the systematic study of alpha-rich freeze-out, the $\alpha\alpha n$ reaction may regulate the production of elements up to A=100 even if it does not lead to the r-process [8, 9]. In the neutron-rich He layer of low-mass asymptotic giant branch (AGB) stars, the $\alpha\alpha n$ reaction might be able to take place below T_9=0.3. This may change the amount of neutrons to determine the abundance of s-process elements [10]. In the inhomogeneous Big-Bang nucleosynthesis, the $\alpha\alpha n$ reaction might contribute to the production of heavier elements beyond A=8 in neutron-rich zones at temperature around T_9=0.1 [11].

Most of nucleosynthesis studies treating the $\alpha\alpha n$ reaction adopt the astrophysical reaction rate from the compilation of CF88 [12]. A more recent evaluation of the ^{9}Be formation rate can be found in the NACRE compilation of the thermonuclear reaction rates [13].

Since the direct measurement of the $\alpha(\alpha n, \gamma)^9$Be reaction is impossible, the experimental efforts to provide information on excited states in ^{9}Be have been made (see [13, 14] and the references therein). A ternary process hardly plays a role in the formation of ^{9}Be. Instead, the reaction reflects nuclear structure of ^{9}Be with large neutron-decay widths of low-lying states in ^{9}Be. The reaction is described by $\alpha + \alpha \rightleftharpoons {}^8$Be(n,$\gamma$)^{9}Be, which takes place during the lifetime of ^{8}Be ($\sim 10^{-16}$ s) in such suitable astrophysical site as the neutrino-driven wind. Therefore, the resonance structure of ^{9}Be near the threshold for ^{8}Be+n at 1.665 MeV is of great importance [15]. It is noted that the reaction $\alpha + n \rightleftharpoons {}^5$He($\alpha$,$\gamma$)^{9}Be with the lifetime of ^{5}He ($\sim 10^{-21}$ s) can make an additional contribution to the formation of ^{9}Be [16, 17].

Recently, a systematic measurement of the ^{9}Be(γ,n)^{8}Be reaction was made with laser-

electron photon beams in the energy range of astrophysical relevance [14]. This study has provided photoneutron cross sections as a function of γ-ray energy. The data enables us to derive the neutron capture cross section of ^{8}Be with the detailed-balance theorem, which is necessary in the calculation of the reaction rate for the ^{9}Be formation. This systematic treatment of all the resonances is preferable in contrast with the preceding treatment which adopted different sources of experimental information on the resonances together with some assumptions.

The brief report [14] provided the reaction rate of $< \alpha\alpha n >$ as a function of temperature. However, the reaction rate was not tabulated, but shown only graphically as a ratio with respect to the NACRE compilation. The temperature range was limited between T_9=0.1 and T_9=10, where only the on-resonant contribution from ^{8}Be was taken into account. In contrast, the NACRE compilation treated a broader temperature range down to T_9=10^{-3} for possible astrophysical applications. At temperatures below T_9=0.028, the effective energy window for the $\alpha\alpha n$ reaction is far below the resonance energy of ^{8}Be. In this case, the off-resonant contribution for the formation of ^{8}Be from $\alpha + \alpha$ becomes important. This contribution was first shown to be important in the determination of the triple alpha reaction in accreting white dwarfs and neutron stars [18].

In this paper, we calculate the reaction rate for the ^{9}Be formation taking into account both on- and off-resonant contributions based on the latest experimental information on photoneutron cross sections for ^{9}Be. It is to be noted that we add data points immediately above the neutron threshold since the brief report [14]. We provide the reaction rate in the wide range of temperatures from T_9=10^{-3} to T_9=10^1 in the analytical fitting formula as well as in the tabular form.

We arrange this article as follows. In section 2, we briefly review the preceding efforts to derive the $\alpha\alpha n$ reaction rate from the point of view of experimental information and experimental methods adopted. In section 3, we describe the photoneutron cross section for ^{9}Be adopted to derive the reaction rate for the neutron capture of ^{8}Be. The description of the experimental method is limited to minimum unless it is associated with added data and a new analysis. In section 4, we explain the theoretical method to derive the $\alpha\alpha n$ reaction rate from

the experimental data. In section 5, we provide the numerical results of the reaction rate in a tabular form and plots. We also provide the fitting formulae of the reaction rate. We compare the result with the reaction rate in the CF88 and NACRE compilations. The article is closed with a summary in section 6.

2   Resonances of ^{9}Be

Fowler, Caughlan, and Zimmerman [19] presented the reaction rate of $\alpha(\alpha n, \gamma)^9$Be in their second volume of *Thermonuclear Reaction Rates* published in 1975 (hereafter referred to as FCZ II). The rate has not been revised in the third volume (1983) [20] of the series and subsequently passed on to the two compilations of Caughlan, Fowler, Harris, and Zimmerman (1985) [21] and of Caughlan and Fowler (1988) [12] (hereafter referred to as CF88) without modification. It was nearly a quarter century after the FCZ II that Angulo *et al.* [13] updated the reaction rate (hereafter referred to as NACRE).

Early measurements of photoneutron cross sections for ^{9}Be were carried out with monochromatic γ rays from radioactive isotopes [22, 23, 24, 25, 26] and with bremsstrahlung [27, 28]. The data of Berman *et al.* exhibit the maximum cross section 1.6 mb at 6 keV above the n + ^{8}Be threshold (E_t = 1.665 MeV) and decrease to 1.2 mb at 40 keV [28]. Parametrizing the photoneutron cross sections by $\sigma_{\gamma n}$ = 1.6 exp(-4E) mb (E in MeV) with E = E_γ - E_t [13] resulted in the CF88 reaction rate $N_A^2 < \alpha\alpha n >$ as

$$N_A^2 \langle \alpha\alpha n \rangle = 2.59 \times 10^{-6} \frac{\exp(-1.062/T_9)}{[T_9^2(1 + 0.344 T_9)]}, \tag{1}$$

where T_9 gives temperature as T = $T_9 \times 10^9$ K and N_A is Avogadro's number. The low energy experimental data were recently investigated in a semi-classical model to derive the $\alpha(\alpha n, \gamma)^9$Be reaction rate [29].

Woosley and Hoffman discussed the reaction rate in a narrow level approximation for two lowest states (the $1/2^+$ and $5/2^-$ states) in the n + ^{8}Be channel. It was pointed out that when the resonance parameters from the (e,e$'$) data of Clerc *et al.* [30] are employed (i.e., E_{x1} = 1.78 ± 0.03 MeV and $\Gamma_{\gamma 1}$ = 0.30 ± 0.12 eV for $1/2^+$ and E_{x2} = 2.44 ± 0.02 MeV and $\Gamma_{\gamma 2}$ = 0.089 ± 0.01 eV for $5/2^-$), the rate is consistent with the CF88 rate to within 30 % in the range T_9

= 1 - 3 [8]. The narrow level approximation holds for the $5/2^-$ state with $\Gamma = 0.77 \pm 0.15$ keV, but not for the $1/2^+$ state with $\Gamma = 217 \pm 10$ keV [15]. In the discussion, the discrepancy in E_{x1} was also pointed out between Ref. [30] and the latest compilation of nuclear physics data [15] which adopted $E_{x1} = 1.684$ MeV ± 7 keV from a different (e,e$'$) data of Kuechler et $al.$ [31].

After the FCZ II, some new measurements of $\sigma_{\gamma n}$ were carried out with both monochromatic γ rays from radioactive isotopes [32] and with bremsstrahlung [33, 34]. An R-matrix fit to the $\sigma_{\gamma n}$ of Fujishiro et $al.$ [32] in one level approximation gave parameters B $= 1.06^{+0.19}_{-0.16}$ mb, ϵ_R $= 192$ keV, and $E_R = 67$ keV [35] which can be converted to B(E1$\downarrow$) $= 0.106^{+0.019}_{-0.016}$ e^{2}fm^2, E_x $= 1.733$ MeV, and $\Gamma \cong \Gamma_n = 227$ keV, respectively. The last quantity was evaluated from $\Gamma_n = 2\sqrt{\epsilon_R(E_\gamma - E_t)}$ with $E_\gamma - E_t = 67$ keV. A major difference between the photonuclear reaction and the electron scattering is that the former B(E1$\downarrow$) [32] is a factor of two lager than the latter one (B(E1$\downarrow$) $= 0.050 \pm 0.020$ [30] and B(E1$\downarrow$) $= 0.054 \pm 0.004$ [31]). According to the Barker's analysis, the main reason for the discrepancy may be due to a potential problem of background subtraction in the electron scattering. Barker pointed out that the (e,e$'$) result may represent not a full but a partial strength of B(E1$\downarrow$).

The NACRE rate of Angulo et $al.$ is based on three states in ^{9}Be, i.e., the $1/2^+$, $1/2^-$, and $5/2^+$ states, neglecting the $5/2^-$ state. Resonance parameters (E_x, Γ_n, and Γ_γ) employed for the $1/2^+$ state were taken from the $\sigma_{\gamma n}$ measurements of Fujishiro et $al.$ [32, 35], where Γ_γ was 0.51 ± 0.10 eV. For the broad $1/2^-$ state at $E_x = 2.78 \pm 0.12$ MeV with $\Gamma = 1080 \pm 110$ keV [15], $\Gamma_\gamma = 1$ W.u. (0.45 eV) for an M1 decay was assumed with a 80 % uncertainty [36]. For the $5/2^+$ state at $E_x = 3.049$ MeV ± 9 keV with $\Gamma = 282 \pm 11$ keV [15], $\Gamma_\gamma = 0.90 \pm 0.45$ eV which is much larger than the (e,e$'$) result (0.30 $\pm$ 0.25 eV) of Clerc et $al.$ was adopted with the increased uncertainty based on the $\sigma_{\gamma n}$ data of Hughes et $al.$ [33].

Recently, Utsunomiya et $al.$ made a new measurement of $\sigma_{\gamma n}$ for ^{9}Be in the range of $E_\gamma =$ 1.78 - 6.11 with quasi-monochromatic γ rays produced by means of inverse Compton scattering of laser photons [14]. The data essentially include all states of astrophysical interest. A least-squares fit to the data was carried out to extract the Breit-Wigner resonance parameters. Using the (γ,n) cross sections, the $\alpha(\alpha$n, $\gamma)^9$Be reaction rate was evaluated. This evaluation

was based only on the resonant contribution to the reaction $\alpha + \alpha \rightleftharpoons {}^8\text{Be}$ with $\Gamma_\alpha = 6.8 \pm 1.7$ eV. Consequently, the reaction rate is valid only at $T_9 > 0.028$ as is the case for the triple alpha reaction [18].

The $5/2^-$ state was treated differently in the NACRE rate and the rate of Utsunomiya *et al.* It was completely omitted in the former, whereas it was taken into account in the latter assuming its 100 % decay to the ${}^8\text{Be}(0)$ + n channel. The $5/2^-$ state in ${}^9\text{Be}$ was investigated in the ${}^7\text{Li}({}^3\text{He,p}){}^9\text{Be}$ reaction [37] and in β decay of ${}^9\text{Li}$ [38] and found to decay 7.5 ± 1.5 % and 6.4 ± 1.2 % to ${}^8\text{Be}(0)$ + n, respectively. It is reported that the $5/2^-$ state decays dominantly to ${}^5\text{He}(0) + \alpha$ [39]. The $5/2^-$ state with $\Gamma = 0.77 \pm 0.15$ keV lies at $E_x = 2.4294$ MeV ± 1.3 keV below the ${}^5\text{He} + {}^4\text{He}$ threshold energy (2.467 MeV). However, since the ground state in ${}^5\text{He}$ has a large width (0.60 ± 0.02 MeV) [15], the state can decay into the low-energy tail of the ground state.

A potential contribution of the ${}^5\text{He}(0) + \alpha$ channel to the reaction rate was investigated by Buchmann [16] where a 5 % branching of the $5/2^-$ state to the n + ${}^8\text{Be}$ decay channel was taken. Summing up all possible contributions through the ${}^5\text{He} + \alpha$ channel not only from the $5/2^-$ state but also from the $1/2^+$ and $1/2^-$ states resulted in a reaction rate that is one order of magnitude smaller than through the n + ${}^8\text{Be}$ channel at high temperatures, $T_9 \geq 2$ (Fig. 9 of Ref. [16]).

In a recent experiment of β-delayed particle decay of ${}^9\text{C}$, a large background continuum in ${}^9\text{B}$ which decays to the ${}^5\text{Li}$ channel was observed above 2.9 MeV [40]. An R-matrix fit revealed that a low energy part of the continuum consists of a tail of the ground state [17]. The charge-symmetry analogue of this background continuum in ${}^9\text{Be}$ may contribute to the $\alpha(\alpha n, \gamma){}^9\text{Be}$ reaction rate. An attempt to estimate the contribution of the analogue background continuum to the $\alpha(\alpha n, \gamma){}^9\text{Be}$ reaction rate through the ${}^5\text{He} + \alpha$ channel was made, showing that it possibly dominates the rate for high temperatures above $T_9 \approx 4$ [17, 41]. This result may be qualitatively consistent with the result of a recent microscopic three-cluster study of photoneutron cross sections for ${}^9\text{Be}$ which showed that the ${}^5\text{He} + \alpha$ channel is of growing importance above $E_\gamma \approx 4$ MeV [42].

In the present paper, we evaluate the $\alpha(\alpha n, \gamma){}^9\text{Be}$ reaction rate through the ${}^8\text{Be}$ + n channel,

including a fractional contribution of the $5/2^-$ state. The contribution through the ^{5}He + α channel is not included because of a lack of sufficient experimental information on the ^{5}He + α channel. Clearly, the evaluation of the stellar reaction rate at the next level must await a new experimental outcome for the decay of relevant states in ^{9}Be through the ^{5}He + α channel (particle- and γ- widths and branching ratios of decays) which is expected in the proposed experiment of β-delayed particle decay of ^{9}Li [16, 17].

3   Photodisintegration of ^{9}Be

3.1   Experiment

We limit a description of the experiment to minimum and concentrate on new facets of the data and data analysis. Many of the details can be found in [14]. The experiment was performed at the National Institute of Advanced Industrial Science and Technology (AIST) which is reorganized from the Electrotechnical Laboratory. Quasi-monochromatic γ-ray beams were generated by means of inverse Compton scattering of YLF: Nd laser photons with $\lambda = 1053$ nm (1.2 eV) from relativistic electrons stored in an accumulator ring TERAS. The energy of the laser-electron photon beams (LEPBs) was varied in the energy range of 1.69 - 6.11 MeV by changing the electron beam energy from 308 to 587 MeV. The LEPBs were collimated into a spot 2 mm in diameter with a 20 cm thick Pb block at 550 cm from the head-on collision point. The beam intensity which gradually decreased with the electron beam current was in the range of 10^5 - 10^4 cps. A 4 cm thick ^{9}Be was irradiated and neutrons were detected with four BF$_3$ counters embedded in a 30 cm polyethylene cube. A BGO detector was used as a flux monitor of the LEPB.

Experimentally two reaction channels of n + ^{8}Be and ^{5}He + α cannot be distinguished. Different cross sections may result depending on the reaction channels because the neutron detection efficiency may be different in the two channels. This complication could occur for the $5/2^-$ state which decays to the two channels, whereas other states are free from such complication because they are known to predominantly decay to the n + ^{8}Be channel [15]. The average energy of neutrons emerging from the decay of the $5/2^-$ state to the two channels was

calculated. The energy of this state is well defined at 2.4294 MeV ($\pm$ 1.3 keV) with $\Gamma = 0.77$ keV ($\pm$ 0.15 keV). When this state decays to the n + ^{8}Be channel at 1.665 MeV, the average laboratory energy of neutrons is 382 keV. On the other hand, this state can decay to the ^{5}He + α channel at 2.467 MeV with the low-energy tail of Γ (^{5}He) = 0.60 MeV ($\pm$ 0.02 MeV). The average energy of neutrons resulting from ^{5}He was calculated to be 156 keV.

Figure 1 shows the detection efficiency of the neutron detector as a function of neutron energy. The efficiency was calibrated with a 265 keV-neutron source of ^{24}NaOH + D_2O and a ^{252}Cf standard source. The energy dependence of the efficiency was calculated with a Monte Carlo code MCNP [43]. The efficiency was 6.62 % at 382 keV and 6.65 % at 156 keV. Thus, the difference in detection efficiency between the two reaction channels is negligible. Cross sections presented in this paper are based on the detection efficiency for the n + ^{8}Be reaction channel.

Figure 2 shows an energy spectrum of the LEPB measured with a high-purity Ge detector. The LEPB has a characteristic low-energy tail that is determined by the electron beam emittance, the laser optics and the collimator size. When the low-energy tail crosses the neutron threshold of ^{8}Be + n (1.665 MeV), not the total but a partial flux of the LEPB is responsible for photodisintegration of ^{9}Be. This occurs for LEPBs whose peak energies are very close to the neutron threshold energy. Previously photoneutron cross sections were presented at energies above 1.78 MeV without flux corrections. As a result, cross sections in the peak region of the $1/2^+$ state were missing in [14].

The flux correction was made for LEPBs by means of a Monte Carlo simulation. Energy spectra of the LEPBs taken with the Ge detector were reproduced with a Monte Carlo code EGS4 [44] by simulating electromagnetic interactions between a LEPB and the Ge detector. The energy distribution of the LEPB which best reproduced the response of the Ge detector is shown by the solid line in Fig. 2.

Figure 3 shows photoneutron cross sections obtained in the present experiment. The flux correction was made for the data in the energy range from the neutron threshold to 2 MeV. These data are plotted at the average energies by the solid circles in the figure. Note that the three data points at 1.69, 1.71, and 1.73 MeV which covered the peak region of the $1/2^+$ state are consistent with the data of Fujishiro *et al.* It was essential to have these data points in a

new analysis because the statistical uncertainty of the Fujishiro data is quite large.

Including all the data with the flux correction, a new least-squares fit was performed to extract the Breit-Wigner parameters for resonance states in ^{9}Be. The same fitting procedure as in [14] was followed using a straight-line cross section ($\sigma = 0.38$ E$_\gamma$ - 1.21 [mb], E$_\gamma$ in MeV) for higher-lying states in the energy region up to 6.1 MeV. The E1 parametrization was used for the positive-parity states ($1/2^+$ and $5/2^+$), while the M1 parametrization for the negative-parity state ($5/2^-$). Due to the fact that the energy spread of the LEPBs was much larger than the total width ($<$ 1 keV) of the $5/2^-$ state, the line shape of the state was not determined experimentally. As a result, only Γ_γ was deduced from the integrated cross section. The best fit is shown by the solid lines. The best fit parameters are listed in Table 1.

It is to be pointed out that there are large differences in B(E1$\downarrow$) and B(M1$\downarrow$) for ^{9}Be states between photodisintegration and electron scattering. While the present B(E1$\downarrow$) for the $1/2^+$ state is consistent with the result of the photodisintegration experiment with radioactive isotopes ($0.106^{+0.019}_{-0.016}$) [32], it is larger by a factor of two than the results of electron scattering (0.050 ± 0.020 [30] and 0.054 ± 0.004 [31]). Similarly, the present B(E1$\downarrow$) for the $5/2^+$ state is about 4 times larger than that (0.010 ± 0.008) from (e, e$'$) [30], whereas the B(M1$\downarrow$) for the $5/2^-$ state is about half that (0.536 ± 0.060) from (e, e$'$) [30].

Regarding the difference for $1/2^+$, Barker previously pointed out a potential problem of background subtraction in electron scattering. As can be seen in the line-shape (Fig. 3), the $1/2^+$ and $5/2^+$ states overlap each other with substantial tails underneath the narrow $5/2^-$ state. The electron scattering strongly enhanced the excitation of the M1 state ($5/2^-$) adjacent to the E1 states ($1/2^+$ and $5/2^+$) [30, 31]. The authors of Ref. [30] realized a background subtraction problem in the discussion of the $1/2^+$ state (Section 5.3 of Ref. [30]), with the statement "Because of the large background and the limited statistical accuracy of this small peak, the contribution of the long tail to be expected from the (γ,n) cross section is not included in the result. Therefore, it is reasonable to make a comparison with the (γ,n) cross section integrated up to 2 MeV only." Indeed, the B(E1$\downarrow$) resulting from the present (γ,n) cross section integrated up to 2 MeV is in good agreement with that given in the electron scattering. Similarly, the B(E1$\downarrow$) for the weakly populated $5/2^+$ state can be underestimated

in the electron scattering for the background problem. This explains, however, the difference only qualitatively which is larger for the $5/2^+$ state (4 times) than for the $1/2^+$ state (2 times).

Regarding the differences for the $5/2^-$ state and the $5/2^+$ state, a broad M1 state ($1/2^-$), which supposedly exists over the 2.5 – 3.5 MeV region [37], complicates the situation. The present least-squares fit did not single out the $1/2^-$ state which was reported to be a broad state at 2.78 MeV with $\Gamma \sim 1$ MeV [15]. If one treats the $1/2^-$ state exactly in the same manner as in the NACRE compilation (E_x = 2.78 ± 0.12 MeV, Γ = 1080 ± 110 keV, Γ_γ = 1 W.u. (0.45 eV)), the peak cross section at 2.78 MeV is found to be 0.066 mb. This cross section is one order of magnitude smaller than the experimental cross section in the corresponding energy region. It is interesting to note that the present Γ_γ for $5/2^+$ (1.24 ± 0.02 eV) is accidentally close to the sum of the Γ_γ's employed in the NACRE compilation for $5/2^+$ (0.90 ± 0.45 eV) and $1/2^-$ (0.45 eV) to within the associated uncertainty. A more quantitative understanding of this energy region is necessary.

3.2 Photoneutron and neutron capture cross sections

We here present analytic formulae to express the cross sections with the resonance parameters which are determined by the least-squares fit described in the previous section.

The photoneutron cross sections for each resonance state of ^{9}Be are given as,

$$\sigma_{\gamma,n}(1/2^+) = 6.654 \times 10^{-2} \bar{E}_\gamma \frac{[181.9(\bar{E}_\gamma - 1665.3)]^{1/2}}{[(\bar{E}_\gamma - 1735.1)^2 + 181.9(\bar{E}_\gamma - 1665.3)]} \text{[mb]}, \tag{2}$$

$$\sigma_{\gamma,n}(5/2^+) = 7.805 \times 10^{-2} \bar{E}_\gamma \frac{274.72}{(\bar{E}_\gamma - 3077.0)^2 + 75471.} \text{[mb]}, \tag{3}$$

$$\sigma_{\gamma,n}(5/2^-) = 3.4616 \times 10^7 \bar{E}_\gamma^{-2} \frac{1}{(\bar{E}_\gamma - 2429.)^2 + 0.14823} \text{[mb]}. \tag{4}$$

Here, the energy of photon, $\bar{E}_\gamma$, is given in unit of keV. In the formulae for the broad positive-parity states ($1/2^+$, $5/2^+$), the energy dependence of the γ-decay width (Γ_γ) is explicitly taken into account;

$$\Gamma_\gamma = \frac{16\pi}{9} \alpha(\hbar c)^{-2} E_\gamma^3 \, \text{B(E1)}, \tag{5}$$

where α is the fine-structure constant. In contrast, Eq. (4) results from the energy-independent Γ_γ for the sharp $5/2^-$ state.

The total cross section of photodisintegration of ^{9}Be is the sum of three contributions given by,

$$\sigma_{\gamma,n} = \sigma_{\gamma,n}(1/2^+) + \sigma_{\gamma,n}(5/2^+) + f_{n^8Be}\,\sigma_{\gamma,n}(5/2^-), \tag{6}$$

where the prefactor f_{n^8Be} is the branching ratio of the $5/2^-$ state to the n + ^{8}Be decay channel. We take a 7 % decay ($f_{n^8Be} = 0.07$) based on the experimental studies [37, 38] to derive the reaction rate. The reaction rate does not change largely even if we assume a 100 % decay ($f_{n^8Be} = 1$) to the n + ^{8}Be decay channel. This point will be discussed later in section 5.

The photoneutron cross section can be converted into the neutron capture cross section of ^{8}Be based on the detailed-balance theorem. The neutron capture cross section, σ_{nBe}, is related with the photoneutron cross section, $\sigma_{\gamma,n}$, by the formula,

$$\sigma_{nBe}(E_n) = \frac{2(2j_a + 1)}{(2j_b + 1)(2j_c + 1)} \frac{k_\gamma^2}{k_n^2} \sigma_{\gamma,n}(E_\gamma), \tag{7}$$

where a, b and c denote ^{9}Be, ^{8}Be and neutron, respectively. The energy, E_n, is the neutron energy with respect to the threshold of n+^{8}Be, defined as,

$$E_n = E_\gamma - 1.6653, \tag{8}$$

in MeV. The wave numbers k_n and k_γ are given, respectively, by,

$$k_n^2 = \frac{2\mu E_n}{\hbar^2}, \tag{9}$$

$$k_\gamma = \frac{E_\gamma}{\hbar c}, \tag{10}$$

where μ is the reduced mass of the n+^{8}Be system. Thus, the neutron capture cross section is given by,

$$\sigma_{nBe}(E_n) = 2.415 \times 10^{-3} \frac{(E_n + 1.6653)^2}{E_n} \sigma_{\gamma,n}(E_\gamma), \tag{11}$$

from the measured photoneutron cross section, Eq. (6). Note that $\bar{E}_\gamma\ (= 10^3 E_\gamma)$ in Eq. (6) is calculated as $E_\gamma = E_n + 1.6653$, through Eq. (8).

4 Theoretical analysis

4.1 $\alpha\alpha n$ reaction rate

We derive the thermal reaction rate of $\alpha(\alpha n, \gamma)^9$Be in two steps through a metastable ^{8}Be. We apply the formulation, which was used to derive the triple alpha reaction by Nomoto *et al.* [18], to the ^{9}Be formation. The same formulation is also employed in the NACRE compilation [13].

The reaction rate $N_A^2 < \alpha\alpha n >$ (i.e. $N_A^2 < \sigma v >^{\alpha\alpha n}$) is calculated by,

$$N_A^2 < \sigma v >^{\alpha\alpha n} = N_A \left(\frac{8\pi}{\mu_{\alpha\alpha}^2} \right) \left(\frac{\mu_{\alpha\alpha}}{2\pi k_B T} \right)^{3/2} \int_0^\infty \frac{\hbar \sigma_{\alpha\alpha}(E)}{\Gamma_\alpha(^8\text{Be}, E)} \exp(-E/k_B T) N_A < \sigma v >^{n^8\text{Be}} E dE, \tag{12}$$

where $\mu_{\alpha\alpha}$ is the reduced mass of the $\alpha + \alpha$ system. E is the energy of $\alpha + \alpha$ with respect to the threshold (the sum of the rest masses of $\alpha + \alpha$). $\sigma_{\alpha\alpha}(E)$ is the cross section for ^{8}Be formation at an energy E, which is, in general, different from the ground-state resonance energy of ^{8}Be, $E_{^8\text{Be}}$. $\Gamma_\alpha(^8\text{Be}, E)$ is the α-decay width of ^{8}Be at an energy E. We describe the ^{8}Be formation and its α decay in the next subsection.

The neutron capture rate of ^{8}Be is calculated by,

$$N_A < \sigma v >^{n^8\text{Be}} = N_A \left(\frac{8\pi}{\mu_{n^8\text{Be}}^2} \right) \left(\frac{\mu_{n^8\text{Be}}}{2\pi k_B T} \right)^{3/2} \int_0^\infty \sigma_{n^8\text{Be}}(E'; E) \exp(-E'/k_B T) E' dE', \tag{13}$$

where $\mu_{n^8\text{Be}}$ is the reduced mass of the n $+$ ^{8}Be system. E' is the energy of n $+$ ^{8}Be with respect to the threshold (the sum of the rest masses of a neutron and a ^{8}Be). Note that this threshold varies with the formation energy E of ^{8}Be. $\sigma_{n^8\text{Be}}(E'; E)$ is the cross section for neutron capture of ^{8}Be at the formation energy E.

We calculate this cross section using the result of Eq. (11) in section 3.2. Since the neutron energy in Eq. (11) is measured from the threshold for n $+$ ^{8}Be, we convert E' to E_n with the ground-state resonance energy $E_{^8\text{Be}}$ by,

$$E_n = E' + E - E_{^8\text{Be}}, \tag{14}$$

to calculate the neutron capture cross section.

4.2 ^{8}Be formation

We calculate the ^{8}Be formation cross section following the prescription of Nomoto *et al.* For details, see Section 2.2.2 of Ref. [18]. The cross section is given by,

$$\sigma_{\alpha\alpha}(E) = \frac{S(E)}{E} \exp[-(E_G/E)^{1/2}], \tag{15}$$

where E_G is the Gamow energy given by,

$$E_G^{1/2} = 0.98948 Z_1 Z_2 A^{1/2} \, \text{MeV}^{1/2}. \tag{16}$$

Here Z_1, Z_2 are the proton numbers of target and projectile nuclei. A is the reduced mass number,

$$A = \frac{A_1 A_2}{A_1 + A_2}, \tag{17}$$

calculated from the mass numbers of target and projectile nuclei A_1, A_2.

The S-factor $S(E)$ is calculated by,

$$S(E) = \frac{0.6566 \, \omega_r}{A} \frac{\Gamma_1(E_r)\Gamma_2(E)}{(E - E_r)^2 + \Gamma(E)^2/4} \exp[(E_G/E_r)^{1/2} + \alpha_l E_r - \alpha_l E)] \, \text{MeV barn}, \tag{18}$$

where E_r is the resonance energy and $\omega_r = [(2J_r + 1)/(2J_1 + 1)(2J_2 + 1)](1 + \delta_{12})$. The energy dependent total decay width $\Gamma(E)$ is calculated by,

$$\Gamma(E) = \Gamma(E_r) \exp[-(E_G/E)^{1/2} - \alpha_l E + (E_G/E_r)^{1/2} + \alpha_l E_r]. \tag{19}$$

Note that $\Gamma_2(E)$ in Eq. (18) cancels out with $\Gamma_\alpha(^8\text{Be}, E)$ in Eq. (12). Taking $l = 0$, the factor α_l is defined by [1],

$$\alpha_{l=0} = \frac{1}{3E_R} \left\{ \frac{K_3(x)}{K_1(x)} - 1 \right\}, \tag{20}$$

where $K_l(x)$ is the modified Bessel function of order l, E_R is given by,

$$E_R = \frac{20.9}{AR^2} \, \text{MeV} \tag{21}$$

with $R = 1.44(A_1^{1/3} + A_2^{1/3})$ fm and x is given by

$$x = 0.525(AZ_1 Z_2 R)^{1/2}. \tag{22}$$

5 Numerical results

5.1 Calculated reaction rate

We numerically integrate Eqs. (12) and (13) with the cross sections Eqs. (11) and (15) to derive the reaction rate $N_A^2 < \alpha\alpha n >$. We provide the calculated data of the reaction rate $N_A^2 < \alpha\alpha n >$ in Table 2. The grid points of temperature is the same as those of the NACRE compilation for comparison.

Figures 4 and 5 display the numerical result of the reaction rate $N_A^2 < \alpha\alpha n >$ as a function of temperature (T_9). For comparison, the reaction rates by Caughlan and Fowler (CF88) [12] and Angulo *et al.* (NACRE) [13] are shown by dashed and dotted curves, respectively.

The difference from the CF88 is apparent at $T_9 \leq 0.028$ due to lack of the off-resonant contribution in CF88. The neglect of the off-resonant contribution leads to the underestimate of the reaction rate below $T_9 = 0.01$ by more than 20 orders of magnitude. The proper treatment of the off-resonant contribution from the metastable ^{8}Be nucleus is, therefore, essential at low temperatures. The difference remains substantial at high temperatures as seen in Figure 5. The CF88 rate is larger than the present rate at $0.028 < T_9 < 3$ and becomes smaller above $T_9 \sim 3$. On the other hand, the NACRE rate is significantly larger than the present rate at low temperatures $T_9 \leq 0.028$ (Fig. 4), whereas it is in good agreement with the present rate at high temperatures $T_9 \geq 0.1$ (Fig. 5).

The ratios of the CF88 rate and the NACRE rate to the present reaction rate are shown in Fig. 6 by the dashed curve and the dotted curve, respectively. The difference of the CF88 from the present rate amounts to a factor of 2 at $T_9 \geq 0.1$. This is because the CF88 is based on the photoneutron cross section of Berman *et al.*, which shows a larger cross section (1.6 mb) peaked at an energy (1.671 MeV) closer to the threshold than the present cross section. At $T_9 \geq 3$, the CF88 rate becomes smaller because it neglects other resonances (mainly the $5/2^-$ state) at higher energies. The NACRE rate is larger by factors 4–12 than the present rate in the low temperature regime ($T_9 < 0.028$). It becomes closer to the present rate in the transitional regime ($T_9 \sim 0.028$) from off-resonance to on-resonance and consistent with the present rate to within $\pm 20\%$ above $T_9 = 0.1$.

The discrepancy between the NACRE rate and the present rate at $T_9 < 0.028$ is attributed to different behaviors of low-energy tails of broad resonances. Presently, the cross section for the $5/2^+$ state is formulated with the energy-dependent Γ_γ as in Eq. (3), while the NACRE compilation adopted energy-independent widths for the same state ($\Gamma_\gamma = 0.90 \pm 0.45$ eV) and, in addition, for the $1/2^-$ state ($\Gamma_\gamma = 1$ W.u. $= 0.45$ eV). As a result, the low-energy tail decreases faster with energy in the present cross section than that in the NACRE compilation.

The $1/2^+$ resonance immediately above the neutron threshold plays an essential role in the reaction rate. The present photoneutron cross section for the $1/2^+$ resonance agrees well with that of Fujishiro *et al.* [32] which was employed in the NACRE compilation. This explains a similarity between the present rate and the NACRE rate at $T_9 \geq 0.1$.

The $5/2^-$ resonance contributes to the reaction rate only at high temperatures. In the current study, we have taken the 7 % decay of the $5/2^-$ state to the n + ^{8}Be channel. To see the sensitivity to the branching ratio, we calculated the reaction rate assuming the 100 % decay ($f_{n^8Be} = 1$ in Eq. (6)). It was found that the 100 % branching does not change the reaction rate below T_9=1 and increases the rate only by 5 % around T_9=10.

5.2   Analytical expressions

We provide the analytical formula which reproduces the numerical result of the reaction rate $N_A^2 < \alpha\alpha n >$ given in Table 2. We fit the numerical data by using the same formulae as those adopted in Table 3 of the NACRE compilation [13]. The reaction rate of the ^{8}Be formation, $N_A < \alpha\alpha >_{formula}$, is expressed by

$$
\begin{aligned}
N_A < \alpha\alpha >_{formula} \;=\; & 2.43 \times 10^9 \, T_9^{-2/3} \exp(-13.490 \, T_9^{-1/3} - (T_9/0.15)^2) \times (1 + 74.5 \, T_9) \\
& + 6.09 \times 10^5 \, T_9^{-3/2} \exp(-1.054/T_9).
\end{aligned} \tag{23}
$$

The fitting formula of the reaction rate $N_A^2 < \alpha\alpha n >$ for $T_9 \leq 0.03$ is parameterized as

$$
N_A^2 < \alpha\alpha n >_{fitting} = N_A < \alpha\alpha >_{formula} \times a_1(1 + a_2 T_9 + a_3 T_9^2 + a_4 T_9^3 + a_5 T_9^4 + a_6 T_9^5), \tag{24}
$$

and for $T_9 > 0.03$ as

$$
N_A^2 < \alpha\alpha n >_{fitting} = N_A < \alpha\alpha >_{formula} \times a_1(1 + a_2 \log_{10} T_9 + a_3 (\log_{10} T_9)^2 + a_4 (\log_{10} T_9)^3), \tag{25}
$$

where a_i are coefficients to be determined. We perform a least-squares fit to the numerical data of Table 2. The best fit formula for $T_9 \leq 0.03$ is

$$
\begin{aligned}
N_A^2 < \alpha\alpha n >_{fitting} &= N_A < \alpha\alpha >_{formula} \times 1.376 \times 10^{-12} \\
&\times (1 - 58.80\, T_9 - 1.794 \times 10^4\, T_9^2 + 2.969 \times 10^6\, T_9^3 \\
&- 1.535 \times 10^8\, T_9^4 + 2.610 \times 10^9\, T_9^5),
\end{aligned}
\tag{26}
$$

and for $T_9 > 0.03$ is

$$
\begin{aligned}
N_A^2 < \alpha\alpha n >_{fitting} &= N_A < \alpha\alpha >_{formula} \times 2.630 \times 10^{-12} \times (1 - 1.359 \log_{10} T_9 \\
&+ 1.995 \times 10^{-1}(\log_{10} T_9)^2 + 5.251 \times 10^{-1}(\log_{10} T_9)^3).
\end{aligned}
\tag{27}
$$

The above formulae reproduce the numerical data of the reaction rate in Table 2 within ~ 20 % deviation.

6   Summary and discussions

We have studied the astrophysical reaction rate for $\alpha(\alpha n, \gamma)^9$Be, which is important in nucleosynthesis under alpha- and neutron-rich environments. The formation of ^{9}Be by this three body reaction plays an essential role to bridge the mass gap at A=8 and to create intermediate-to-heavy mass nuclei starting from light elements. This reaction rate influences largely the alpha-rich freeze-out followed by the r-process nucleosynthesis in neutrino-driven winds and possibly other nucleosynthesis in various astrophysical sites.

We adopted the latest experimental data on the photodisintegration of ^{9}Be taken with laser-electron photon beams. This experiment covered all resonance states of astrophysical importance in ^{9}Be. We added data points near the neutron threshold with the flux correction for incident photons and updated the least-squares analysis of extracting resonance parameters.

We numerically calculated the thermal average of cross sections for the formation of ^{9}Be via the metastable ^{8}Be, i.e., $\alpha + \alpha \rightleftharpoons {}^8Be(n,\gamma)^9$Be. We took into account both off-resonant and on-resonant contributions from the ground state in ^{8}Be. The off-resonant contribution, which was not included in the previous brief report [14] on the photodisintegration experiment, becomes important at low temperatures below $T_9 = 0.028$.

We have provided the reaction rate in the wide temperature range from $T_9=10^{-3}$ to $T_9=10^1$ both in a tabular form and in analytic formulae. The calculated reaction rate is compared with the reaction rates of the CF88 and the NACRE compilations. The CF88 rate, which is invalid at $T_9 \leq 0.028$ due to lack of the off-resonant contribution, differs from the present reaction rate by a factor of 2 at high temperatures $T_9 \geq 0.1$. The NACRE rate is 4–12 times larger than the present reaction rate at low temperature ($T_9 < 0.028$) and becomes closer to the present rate in the transitional temperature region from off-resonant to on-resonant processes. The NACRE rate is consistent with the present rate at $T_9 \geq 0.1$ to within $\pm 20\%$. Because of the systematic treatment of photoneutron cross sections obtained from the dedicated experiment, we would like to recommend to use the new reaction rate for possible astrophysical problems.

It is worthwhile mentioning possible impacts of the new reaction rate on modeling nucleosynthesis in various astrophysical sites. The production of seed elements in the neutrino-driven wind and the alpha-rich freeze-out scenarios can be enhanced due to the slight increase of the reaction rate at $T_9 > 3.5$. This may lead to a slightly smaller neutron-to-seed ratio at the onset of r-process, and hence make an appreciable influence on the entropy condition and expansion dynamics of the neutrino-driven wind [4]. Kajino et $al.$ have recently studied the sensitivity of the r-process yields to the $\alpha(\alpha n, \gamma)^9$Be reaction rate, and found that a factor of two larger rate would change the final r-process abundances drastically in rapid expansion models of the neutrino-driven wind [45]. These possible implications should be studied in detail by using the present new reaction rate. It is to be clarified quantitatively if the $\alpha(\alpha n, \gamma)^9$Be reaction path still predominates the seed production and to what extent the final r-process yields may change by including the present reaction rate and also newly-identified competing reactions $\alpha(t, \gamma)^7$Li$(n, \gamma)^8$Li$(\alpha, n)^{11}$B [6, 7] in the nuclear reaction network.

It is also postulated theoretically that the production of ^{9}Be in the He layer of AGB stars may change the neutron-rich environment required for the s-process nucleosynthesis. Once proton mixing into C-rich He layer could occur either in the interpulse phase [46, 47] or in the thermal pulse phase [10] of the AGB stars, the reignition of H-burning proton capture on abundant ^{12}C would form ^{13}C. Temperature might exceed $T_9 = 0.09$ so that ^{13}C$(\alpha, n)^{16}$O provides plenty of free neutrons. Since this neutron production could occur in the He layer, the

$\alpha(\alpha n, \gamma)^9$Be reaction may follow and play a role of neutron-poison which regulates the s-process nucleosynthesis. As the burning time scale of $\alpha\alpha n$ depends strongly on the local neutron density and temperature, it is highly desirable to calculate precise profile of the neutron exposure and the temperature distribution in order to identify above theoretical speculation. Note that, should $\alpha(\alpha n, \gamma)^9$Be reaction occur in such an environment of AGB stars, it is hard to observe ^{9}Be because ^{9}Be is easily destroyed by the (p, α) reaction in the next thermal pulse.

Another neutron-rich site in cosmological nucleosynthesis is baryon inhomogeneous Big-Bang Universe [11]. In segregated fluctuations of neutron and proton number-density distributions it is identified that the ^{7}Li$(n, \gamma)^8$Li$(\alpha, n)^{11}$B and ^{7}Li$(t, n)^9$Be reactions are the most viable nuclear flows to produce intermediate-to-heavy mass nuclei in the Big-Bang nucleosynthesis [48, 49, 50]. It should be studied theoretically if the $\alpha(\alpha n, \gamma)^9$Be reaction can be an alternative flow path or a competing reaction with those identified previously.

The $\alpha(\alpha n, \gamma)^9$Be stellar reaction rate was evaluated in a more consistent manner, where the systematic experimental data of photodisintegration of ^{9}Be was used, than in the preceding compilations [12, 13]. As of the present evaluation, however, there still remains some uncertainty regarding the contribution from the ^{5}He $+ \alpha$ channel due to a lack of experimental information on low-lying states in ^{9}Be. A further experimental investigation with emphasis on the ^{5}He $+ \alpha$ configuration is advisable.

Acknowledgment

References

[1] E. M. Burbidge, G. R. Burbidge, W. A. Fowler and F. Hoyle, Rev. Mod. Phys. **29** (1957) 547.

[2] B. S. Meyer, G. J. Mathews, W. M. Howard, S. E. Woosley and R. D. Hoffman, Astrophys. J. **399** (1992) 656.

[3] S. E. Woosley, J. R. Wilson, G. J. Mathews, R. D. Hoffman and B. S. Meyer, Astrophys. J. **433** (1994) 229.

[4] K. Otsuki, H. Tagoshi, T. Kajino and S. Wanajo, Astrophys. J. **533** (2000) 424.

[5] K. Sumiyoshi, H. Suzuki, K. Otsuki, M. Terasawa and S. Yamada, Publ. Astron. Soc. Japan **52** (2000) 601.

[6] M. Terasawa, K. Sumiyoshi, T. Kajino, I. Tanihata, G. J. Mathews and K. Langanke, Nucl. Phys. **A688** (2001) 581c.

[7] M. Terasawa, K. Sumiyoshi, T. Kajino, G. J. Mathews and I. Tanihata, Astrophys. J. **562** (2001) 470.

[8] S. E. Woosley and R. D. Hoffman, Astrophys. J. **395** (1992) 202.

[9] W. M. Howard, S. Goriely, M. Rayet and M. Arnould, Astrophys. J. **417** (1993) 713.

[10] N. Iwamoto, T. Kajino, G. J. Mathews, M. Fujimoto and W. Aoki, submitted to ApJ (2001).

[11] M. Orito, T. Kajino, R. N. Boyd and G. J. Mathews, Astrophys. J. **488** (1997) 515.

[12] G. R. Caughlan and W. A. Fowler, At. Data Nucl. Data Tables **40** (1988) 283.

[13] C. Angulo *et al.*, Nucl. Phys. **A656** (1999) 3.

[14] H. Utsunomiya, Y. Yonezawa, H. Akimune, T. Yamagata, M. Ohta, M. Fujishiro, H. Toyokawa and H. Ohgaki, Phys. Rev. **C63** (2001) 018801.

[15] F. Ajzenberg-Selove, Nucl. Phys. **A490** (1988) 1.

[16] L. Buchmann, in Proceedings of International Symposium on Origin of matter and evolution of galaxies, 1997, ed. S. Kubono, T. Kajino, K. Nomoto and I. Tanihata, (World Scientific, Singapore, 1998) p.142.

[17] L. Buchmann, E. Gete, J.C. Chow, J.D. King and D.F. Measday, Phys. Rev. **C63** (2001) 034303.

[18] K. Nomoto, F.-K. Thielemann and S. Miyaji, Astron. Astrophys. **149** (1985) 239.

[19] W.A. Fowler, G.R. Caughlan and B.A. Zimmerman, Ann. Rev. Astron. Astrophys. **13** (1975) 69.

[20] M.J. Harris, W.A. Fowler, G.R. Caughlan and B.A. Zimmerman, Ann. Rev. Astron. Astrophys. **21** (1983) 165.

[21] G.R. Caughlan, W.A. Fowler, M.J. Harris and B.A. Zimmerman, Atomic Data and Nuclear Data Tables **32** (1985) 197.

[22] B. Russel *et. al.*, Phys. Rev. **73** (1948) 545.

[23] B. Hamermesh and C. Kimball, Phys. Rev. **90** (1953) 1063.

[24] R.D. Edge, Nucl. Phys. **2** (1956/57) 485.

[25] J.H. Gibbons *et. al.*, Phys. Rev. **114** (1959) 1319.

[26] W. John and J.M. Prosser, Phys. Rev. **163** (1967) 958.

[27] M.K. Jakobson, Phys. Rev. **123** (1961) 229.

[28] B.L. Berman, R.L. Van Hemert and C.D. Bowman, Phys. Rev. **163** (1967) 163.

[29] V.D. Efros, H. Oberhummer, A. Pushkin and I.J. Thompson, Eur. Phys. J. **A1** (1998) 447.

[30] H.-G. Clerc *et. al.*, Nucl. Phys. **A120** (1968) 441.

[31] G. Kuechler *et. al.*, Z. Phys. **A326** (1987) 447.

[32] M. Fujishiro *et. al.*, Can. J. Phys. **60** (1982) 1672; ibid. **61** (1983) 1579.

[33] R.J. Hughes *et al.*, Nucl. Phys. **A238** (1975) 189.

[34] A.M. Goryachev, G.N. Zalesny and I.V. Pozdnev, Izvestiya RAN, Seriya Fizicheskaya **56** (1992) 159.

[35] F.C. Barker, Can. J. Phys. **61** (1983) 1371.

[36] P. Descouvemont, Phys. Rev. **C39** (1989) 1557.

[37] P.R. Christensen and C.L. Cocke, Nucl. Phys. **89** (1966) 656.

[38] Y.S. Chen, T.A. Tombrello and R.W. Kavanagh, Nucl. Phys. **A146** (1970) 136.

[39] D. Rendic, Nucl. Phys. **A178** (1971) 40.

[40] E. Gete *et. al.*, Phys. Rev. **C61** (2000) 064310.

[41] L. Buchmann (private communication).

[42] P. Descouvemont, Eur. Phys. J. **A12** (2001) 413.

[43] J.F. Briesmeister, MCNP, A General Monte Carlo N-Particle Transport Code, Version 4B, Los Alamos National Laboratory, 1997.

[44] W.R. Nelson, H. Hirayama and W.O. Roger, *The EGS4 Code Systems*, SLAC-Report-265, 1985.

[45] T. Kajino, S. Wanajo and G. J. Mathews, Nucl. Phys. **A704** (2002) 165.

[46] R. Gallino *et al.*, Astrophys. J. **497** (1998) 388.

[47] M. Busso, R. Gallino and G. J. Wasserburg, Ann. Rev. Astron. Astrophys. **37** (1999) 239.

[48] J. H. Applegate, C. Hogan and R. J. Scherrer, Astrophys. J. **329** (1988) 572.

[49] T. Kajino and R. N. Boyd, Astrophys. J. **359** (1990) 267.

[50] R. N. Boyd, Nucl. Phys. **A693** (2001) 249.

Table 1: Resonance parameters deduced in the present experiment.

I^π	$X\lambda$	E_R	$B(X\lambda\downarrow)$	Γ_γ	Γ_n
		[MeV]	E1:$[e^2fm^2]$	[eV]	[keV]
			M1:$[(e\hbar/2Mc)^2]$		
$1/2^+$	E1	1.735 ± 0.003	0.104 ± 0.002	0.568 ± 0.011	225 ± 12
$5/2^-$	M1	2.43	0.295 ± 0.072	0.049 ± 0.012	
$5/2^+$	E1	3.077 ± 0.009	0.0406 ± 0.0007	1.24 ± 0.02	549 ± 12

Table 2: The thermal reaction rate $N_A^2 < \alpha\alpha n >$ at representative temperatures.

| T_9	rate	T_9	rate
0.001	1.10E-59	0.14	3.35E-08
0.002	6.30E-48	0.15	4.96E-08
0.003	3.12E-42	0.16	6.92E-08
0.004	1.21E-38	0.18	1.18E-07
0.005	4.31E-36	0.2	1.78E-07
0.006	3.81E-34	0.25	3.47E-07
0.007	1.36E-32	0.3	5.06E-07
0.008	2.62E-31	0.35	6.29E-07
0.009	3.19E-30	0.4	7.13E-07
0.01	2.75E-29	0.45	7.62E-07
0.011	1.81E-28	0.5	7.83E-07
0.012	9.63E-28	0.6	7.73E-07
0.013	4.30E-27	0.7	7.25E-07
0.014	1.66E-26	0.8	6.62E-07
0.015	5.68E-26	0.9	5.97E-07
0.016	1.75E-25	1	5.36E-07
0.018	1.30E-24	1.25	4.06E-07
0.02	7.33E-24	1.5	3.12E-07
0.025	2.45E-22	1.75	2.44E-07
0.03	2.98E-19	2	1.95E-07
0.04	1.36E-15	2.5	1.32E-07
0.05	1.98E-13	3	9.61E-08
0.06	5.20E-12	3.5	7.39E-08
0.07	5.15E-11	4	5.94E-08
0.08	2.79E-10	5	4.20E-08
0.09	1.01E-09	6	3.19E-08
0.1	2.79E-09	7	2.54E-08
0.11	6.29E-09	8	2.07E-08
0.12	1.22E-08	9	1.72E-08
0.13	2.12E-08	10	1.45E-08
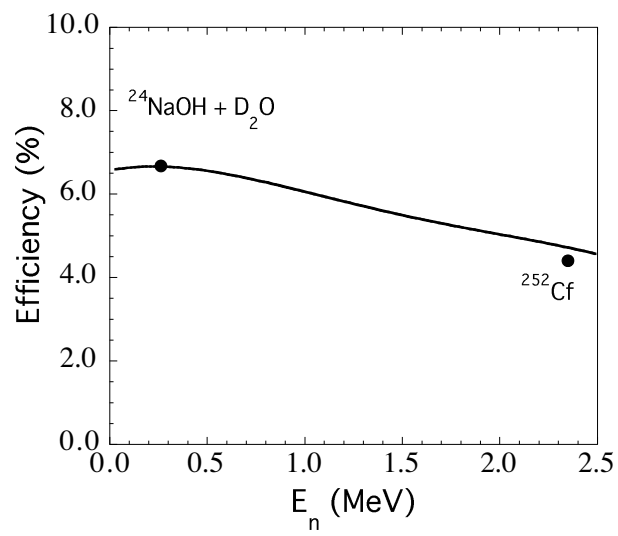
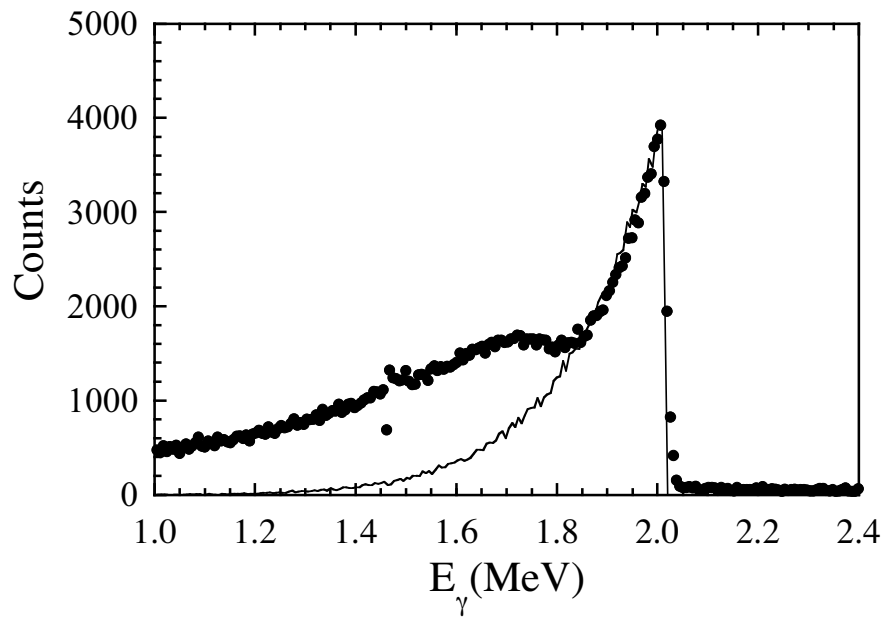Figure 1: Neutron detection efficiency as a function of neutron energy.

Figure 2: Energy distribution of the laser-electron photon beam measured with a high-purity Ge detector. The energy distribution, which best reproduces the response of the Ge detector, is shown by the solid curve.
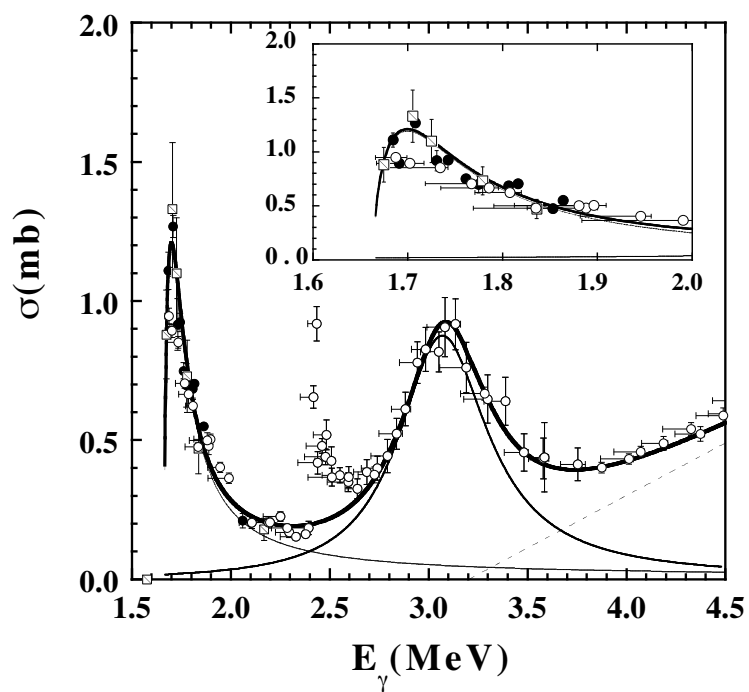
Figure 3: Photoneutron cross sections for ^{9}Be. A low-energy portion is magnified in an inset. The data below 2 MeV are corrected for the γ-ray flux responsible for the photodisintegration. The corrected data are shown by the solid circles. The data at the three lowest energies (1.69, 1.71, 1.73 MeV) near the neutron threshold are consistent with the data of a radioactive isotope measurement (slashed squares) [32] as seen in the inset. The best least-squares fit is shown by the solid lines (thick solid line for sum, thin solid lines for breakdown).
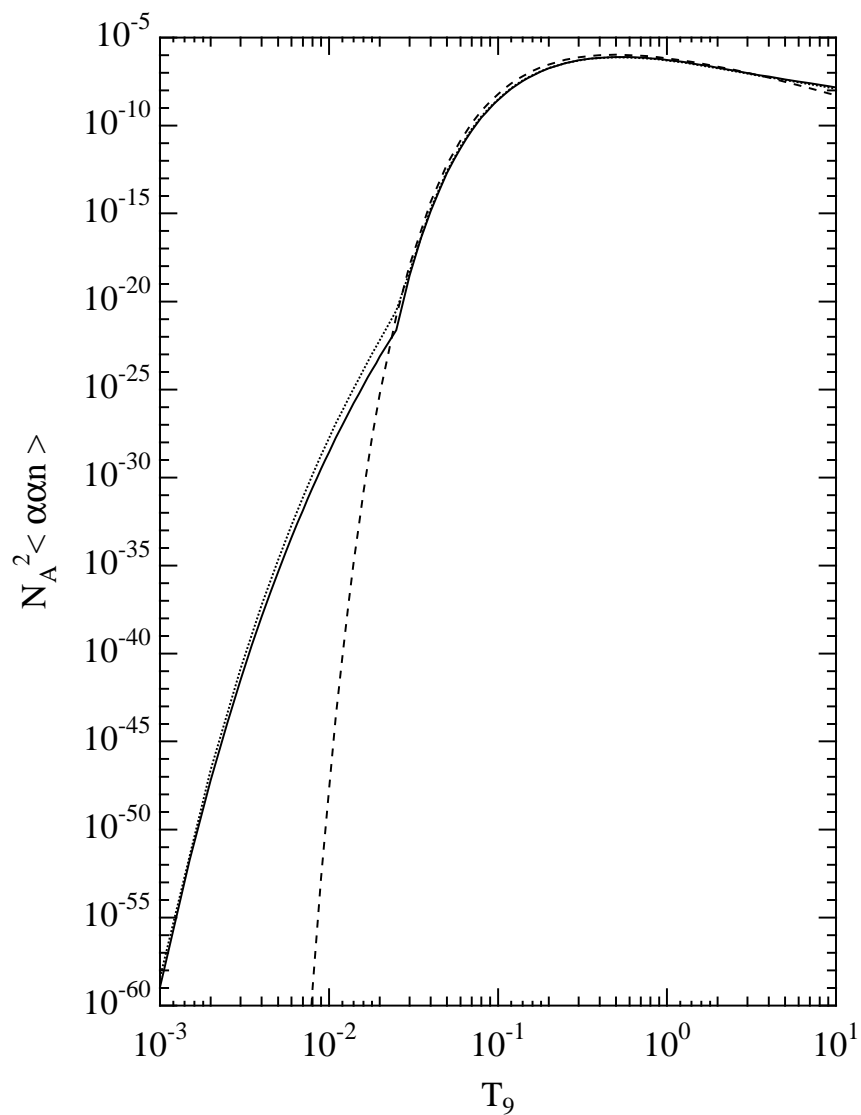
Figure 4: The reaction rate $N_A^2 < \alpha\alpha n >$ in the present study is shown by the solid curve as a function of temperature. The reaction rates by CF88 [12] and NACRE [13] are shown by dashed and dotted curves, respectively.
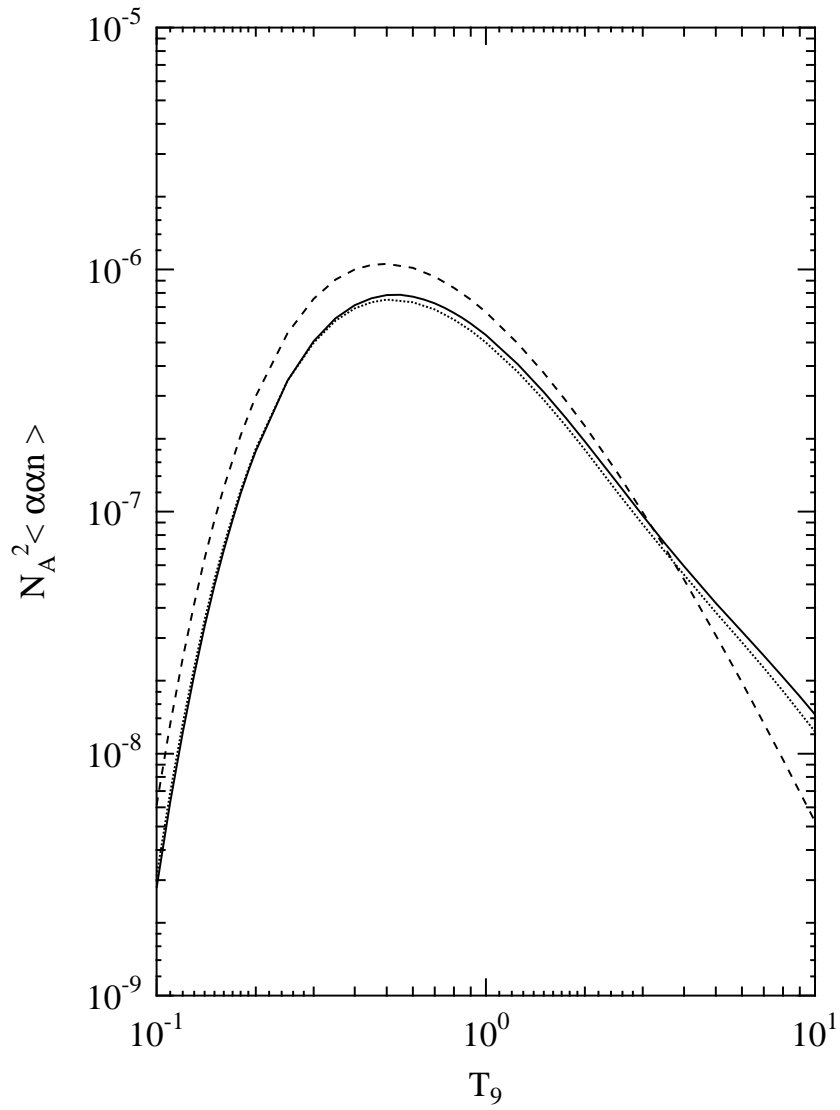
Figure 5: The zoom up of Fig. 4 for a high temperature range. The reaction rates $N_A^2 < \alpha\alpha n >$ are shown as functions of temperature between $T_9 = 10^{-1}$ and $T_9 = 10$ with the same notation as in Fig. 4.
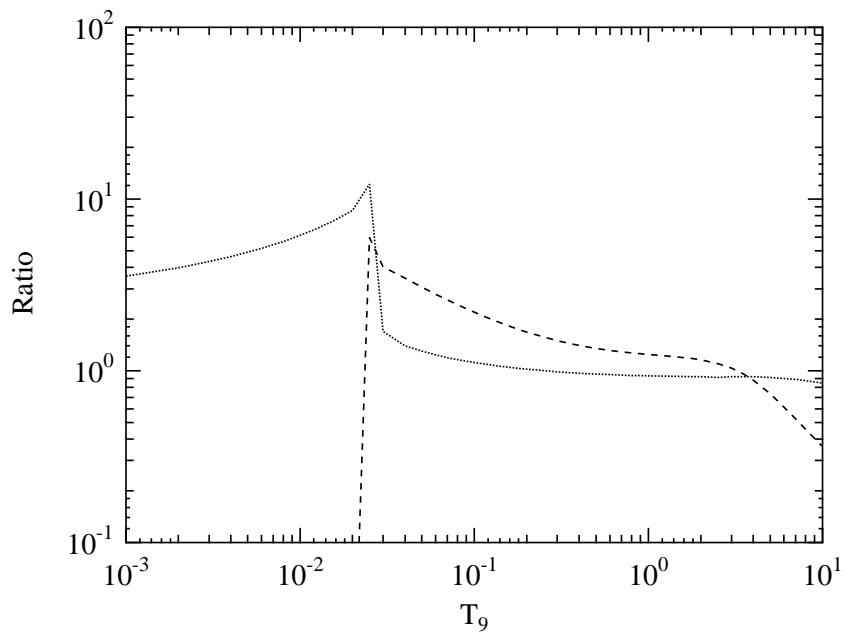
Figure 6: The ratios of the reaction rate $N_A^2 < \alpha\alpha n >$ of the CF88 and NACRE compilations to the present reaction rate are shown by dashed and dotted curves, respectively, as functions of temperature.